pH and anion effects on Cu-phosphate interfaces for CO electroreduction

Paula Sebastián-Pascual, Amanda S. Petersen, Alexander Bagger, Jan Rossmeisl, and María Escudero-Escribano**

Department of Chemistry, University of Copenhagen, Universitetsparken 5, 2100 Copenhagen, Denmark

*Corresponding author:

E-mail: maria.escudero@chem.ku.dk

E-mail: alexander@chem.ku.dk

ABSTRACT

Cu electrodes are promising materials to catalyze the conversion of CO_2 and CO into renewable fuels and valuable chemicals. However, detailed description of the properties of the Cu-electrolyte interface is still crucial to reach a complete understanding of the CO reduction mechanism. Herein, we have investigated the interfacial properties of Cu(111) and Cu(100) in phosphate buffer solutions at different pH conditions and in presence of CO. Ab initio molecular simulations of the Cu-electrolyte interface were combined with voltammetric experiments carried out on Cu(100) and Cu(111) single-crystalline electrodes. Combining multiple cyclic voltammograms on Cu single crystals across the whole pH scale with simulations allows for an in-depth insight into the stability of specifically adsorbed HPO_4* from the electrolyte. We show that the adsorption strength of phosphate species on the different Cu facets affects the potential range at which CO poisons the surface, thus evidencing that the properties of the Cu-electrolyte interface controls the potential range for CO reduction on Cu. This combination of systematic experimental and theoretical analysis across the pH scale is a robust method to gain fundamental structural insight of electrochemical interfaces.

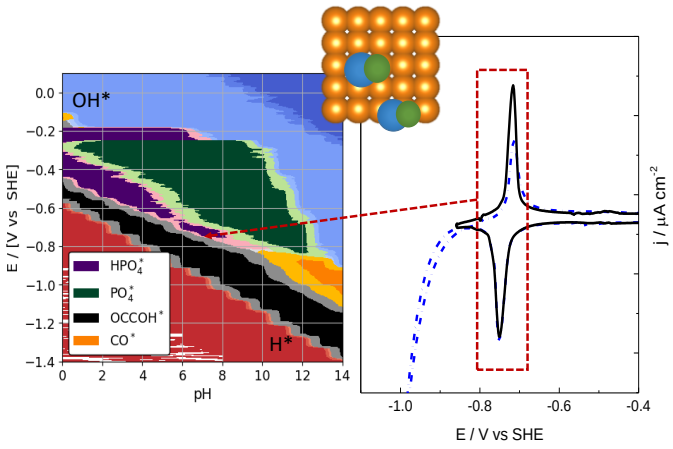

Table of contents graphic

Introduction

Selective and efficient conversion of greenhouse gases such as carbon dioxide (CO_2) into green fuels and chemicals is one of the most important technological and environmental challenges that the society is currently facing.[1–3] Electrocatalytic CO_2 reduction (CO_2RR) is a sustainable alternative to convert CO_2 into renewable fuels and valuable chemicals, allowing for the transition to a decarbonized scheme of energy.[4–6] Up to date, copper is the only pure metal catalyst that can reduce CO_2 beyond carbon monoxide (CO), producing a wide range of fuel alcohols and hidrocarbons.[7–9] In parallel, studies dedicated to investigate the CO reduction reaction on Cu have provided indirect insights for deeper understanding of the CO_2RR.[10–15] The pioneering work by Hori and co-workers on electrocatalytic CO reduction on Cu in the 80s[10,16] have inspired our community for the search of a rational explanation of the reaction mechanism, that continuous to be a focus of debate. In particular, the use of model Cu surfaces such as single-crystalline electrodes, has represented a progress in the understanding of both the CO_2RR and the CORR, allowing to find the relations between electrocatalytic performance, surface structure and electrolyte effects.[12,13,17–24]Aiming to shed lights into the parameters governing the different reactivity towards multi-carbon products, Bagger et al. performed ab initio molecular dynamics to simulate the structure of the electrified interface Cu-aqueous electrolyte for CO reduction.[22,25,26] They suggested that the potential range at which the CO* or OC-COH* dimer intermediate is stable on <100> facets is conditioned by the properties of the Cu-electrolyte interface. In particular, in electrolytes containing anions that specifically adsorb on Cu, such as bicarbonate or phosphate solutions, the anion poisoning the surface controls the onset potential for the formation of C_2H_4, in agreement with previous experiments.[12]

There is a large number of reports that have analyzed electrolyte effects on the CO or CO_2 reduction,[6,14,23,27] as well as the effect of the local pH change on the catalytic performance of Cu catalysts. The latest is particularly relevant as the interfacial pH affects the product distribution on the CO reduction.[27–30] Thus, assessing the effect of both the solution pH and specific anion adsorption on the minimum required potential for the CO or its intermediates to remain stable on Cu single crystalline electrodes is essential for detailed description of the CORR.[12,22,31] Noteworthy, both pH and electrolyte effects have been widely investigated in other electrocatalytic reactions of interest, such as the oxygen reduction reaction on Pt,[32–35] evidencing the key role of the pH and selected electrolyte while assessing the performance of an electrocatalytic reaction. In the particular case of the CORR on Cu, Hori and co-workers investigated the effect of the pH on the adsorption of CO on different Cu single-crystalline surfaces and at low temperature.[31,36,37] They observed that CO weakly adsorbs on Cu, providing a very singular voltammetric feature which potential value depends on surface orientation, employed electrolyte and pH bulk solution. Voltammetric CO displacement technique serves to, experimentally, monitor the presence of adsorbed CO on the surface. Recently, we analyzed the voltammetric features of Cu(111) in different electrolytes and under the presence of CO;[23] our work showed that the main voltammetric structure-sensitive features are highly sensitive to the electrolyte, but also to the presence of CO in the interfacial region.[38,39]

Herein, we combine ab initio molecular dynamics (AIMD) simulations with cyclic voltammetry carried out on Cu(100) and Cu(111) single-crystalline electrodes, to shed lights into the Cu | electrolyte interface properties, and their effect on the onset potential of the CORR. Both simulations and voltammetric experiments were conducted on Cu(111) and Cu(100) in contact with phosphate buffer electrolytes, covering the whole pH scale. This study provides rational

description of the Cu-electrolyte interfacial properties, and show that both pH and electrolyte anions play a key role in controlling the potential windows for electrocatalytic CO reduction.

Results

Cyclic voltammograms (CVs) of both Cu(100) and Cu(111) | 0.1M phosphate solution interface in presence of CO were assessed. Figure 1A shows the voltammogram windows of Cu(100) in contact with CO-saturated phosphate solutions. The recorded CVs across the whole pH range display a quasi-reversible pair of peaks located in the low potential window, *i.e*. close to the solvent and CO co-reduction potential limit (Fig. 1A, potential range between -0.65 V and -0.9 V vs SHE). These voltammetric features correspond to weakly adsorbed CO that replaces the phosphate anions adsorbed on the surface by means of the CO-displacement technique. These results are in agreement with earlier work by Hori and co-workers.[36] Notably, these peaks shift to more negative potential values by increasing the pH of the solution in the standard hydrogen electrode (SHE) scale, showing the pH influence on the voltammetric curves. On the other hand, the hydrogen evolution reaction (HER) or on the surface slightly reduces the reversibility of the CO-anodic peak (see blue line, Fig. 1A), which shifts to more positive potential values. This is likely due to surface restructuration or reconstruction induced by the HER, which affects the voltammetric profile.[40–42] The irreversibility on the peaks is reduced by shortening the potential window (black lines, Fig. 1A). In contrast to CVs recorded in presence of CO, blank CVs of Cu(100) do not display any feature in the pseudocapacitive region in acidic and neutral pH (see Fig S1B from the supporting information (S.I.) material, potential range between -0.2 V to -0.9 V vs SHE, pH<8). The absence of voltammetric features is due to the fact that phosphate adsorption in the blank CV of Cu(100)

overlaps with the HER currents.[31] Under the presence of CO, the characteristic CO-displacement peak appears because the CO poisons the surface, broadening the potential window. In contrast, at alkaline enough pH, the Cu(100) blank CV shows a quasi-reversible peak which is related to the phosphate adsorption on the surface (Fig S1B, potential range between -0.94 V to -1.00 V vs SHE, pH > 8). The presence of CO in solution slightly shifts the phosphate peak to higher potentials, indicating that CO adsorbs on the surface at potentials close to the phosphate desorption potential region.

Figure 1B shows the potential windows of the Cu(111) | 0.1M phosphate at different pH and under the presence of CO. The short potential windows (black line, Fig. 4B) display the quasi-reversible pair of peaks on this crystallographic orientation, and related with the CO adsorption on Cu(111) (peaks are located in the potential region between -0.53 V and -0.70 V vs SHE). [23] Unlike Cu(100), the blank CVs recorded on Cu(111) display the pair of peaks, addressed to adsorbed phosphate, at low pH up to 4 (Fig. S4B, potential region between -0.55 V to -0.72 V vs SHE). This is because, on Cu(111), phosphate desorption occurs at considerable higher potentials well separated from the HER potential limit. As evidenced in Figure 1B, the presence of CO in solution modifies the main voltammetric features of the blank CVs,[23] and slightly shift the phosphate peak towards more positive potential values due to the weak CO adsorption on Cu(111). Importantly, broad potential windows (Fig. 1A blue lines), *i.e.*, scanning to more negative potential that the onset of the HER, highly affect the voltammetric profiles in the anodic scan (potential limits ranging between -0.85 V to -1.4 V vs SHE by increasing the pH from 4 to 12). In particular, both the anodic CO and phosphate peaks (Fig 4 and Fig S1B, blue lines) are considerably shifted to more positive potentials. The effect of the HER or solvent co-reduction on the voltammetric profiles of Cu(111) is considerably stronger than on Cu(100), which surface remain less altered by the selected

potential limits. This shows that Cu(111) is highly sensitive to undergo surface changes under reduction conditions, as we have discussed in our previous report.[23] The surface restructuring also takes places in the absence of CO, being an intrinsic behavior of the (111) orientation (Fig S1B), which origin remains unknown.

Importantly, the charge under the voltammetric peak remains constant with the pH on both Cu(100) and Cu(111), and the presence of CO does not modify this value. The charge value approaches to 45-55μC cm^{-2} on Cu(100), and to 50-60 μCcm^{-2} on Cu(111), in agreement with previous works (Fig S2).[31,43] The anion coverage, assuming one electron transfer, would be between 0.25 and 0.3 monolayer on both surfaces, which is considerably low. The calculated charges through integrated voltammetric peaks suggest that there are uncertainties in the estimation of the real surface coverage through charge coverages on the surface.

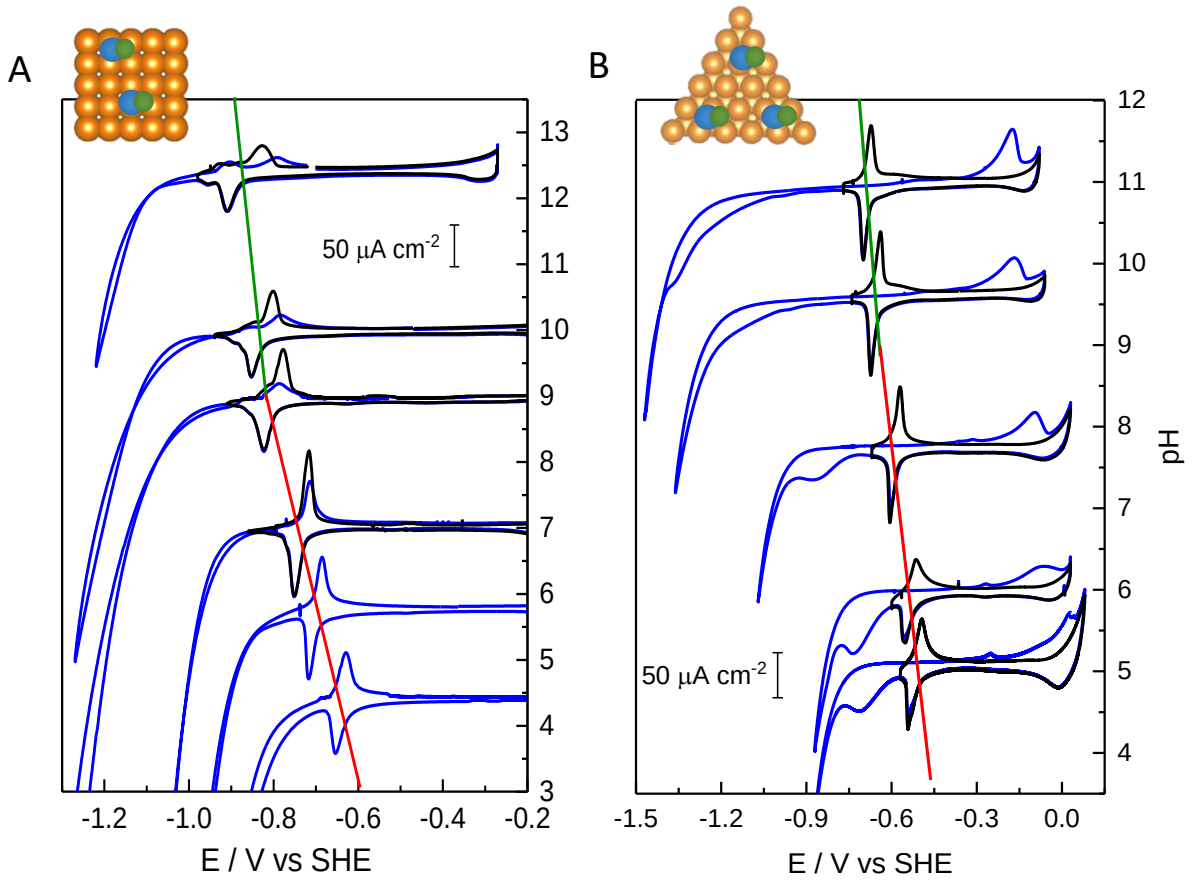

Figure 1: Plot of the cyclic voltammograms of the Cu(hkl) | CO-saturated 0.1 M phosphate buffer interface as a function of the pH (right axis). Scan rate: 50mV/s. A) Cu(100), B) Cu(111). Red and green solid line cross the CO peak at each pH. Blue and black CVs corresponds to long and short potential windows, respectively.

To analyze in detail the effect of the pH on the onset potential of CO adsorption on Cu-single crystalline electrodes, we have plotted the potential average value between anodic peak (E_a) and cathodic peak(E_c) of the CO-displacement voltammetric feature, i.e. ($\frac{Ea+Ec}{2}$). We have extracted the CO-peak potential values from the voltammetric data recorded at narrow potential windows (Fig. 1A, black lines). The averaged potential peak value is assumed to be close to the equilibrium

potential of the CO adsorption on both Cu surfaces (Fig. S3).[31] The potential peak shift with the pH is about 36 mV pH^{-1} on Cu(111) (Fig. 1B, black circles) and 33 mV pH^{-1} on Cu(100) (Fig 2A, blue squares).[31] In contrast, in alkaline media this trend changes, and the potential shift with the pH is more flattered on both surfaces. The obtained slope is about 15 mV per pH unity on Cu(100) and 20mV on Cu(111). Figure 2A clearly shows that CO-peak values on Cu(111) appears allocated at more positive potential values than on Cu(100), which is likely due to phosphate poisons less strong <111> facets than <100> facets.

To get a deeper insight into the phosphate poisoning effect, we have compared the CVs of both Cu(100) and Cu(111) in phosphate blank solutions at high pH with the CVs obtained in the presence of CO(Fig. 2B). Here, we have plotted the cathodic potential peak of both Cu(111) and Cu(100) from either blank phosphate solutions or solutions with CO (Fig 2C). We have selected the potential of the cathodic peak (E_c) because the blank CVs of Cu(100) loses symmetry in the anodic scan at pH < 12 due to overlapping with the HER at these pH (See Fig. S1A). Red symbols represent the phosphate peak in the blank solutions, while black symbols are the CO peaks obtained from the CO-saturated solutions (Fig 2C). The potential difference between phosphate and CO peaks on Cu(111) is small, about 30mV, supporting that CO weakly adsorbs on this surface. In contrast, on Cu(100), this potential difference between phosphate and CO peaks) is considerable higher, about 100 mV (Fig. 2B and C). This suggests that CO possibly adsorbs stronger on Cu(100) than on Cu(111). Despite that, the CO peaks appear at more negative potential values on Cu(100) than on Cu(111), which indicates that the strong adsorption of phosphate on both Cu(100) and Cu(111) is the main parameter controlling the potential windows for CO adsorption on the surface.

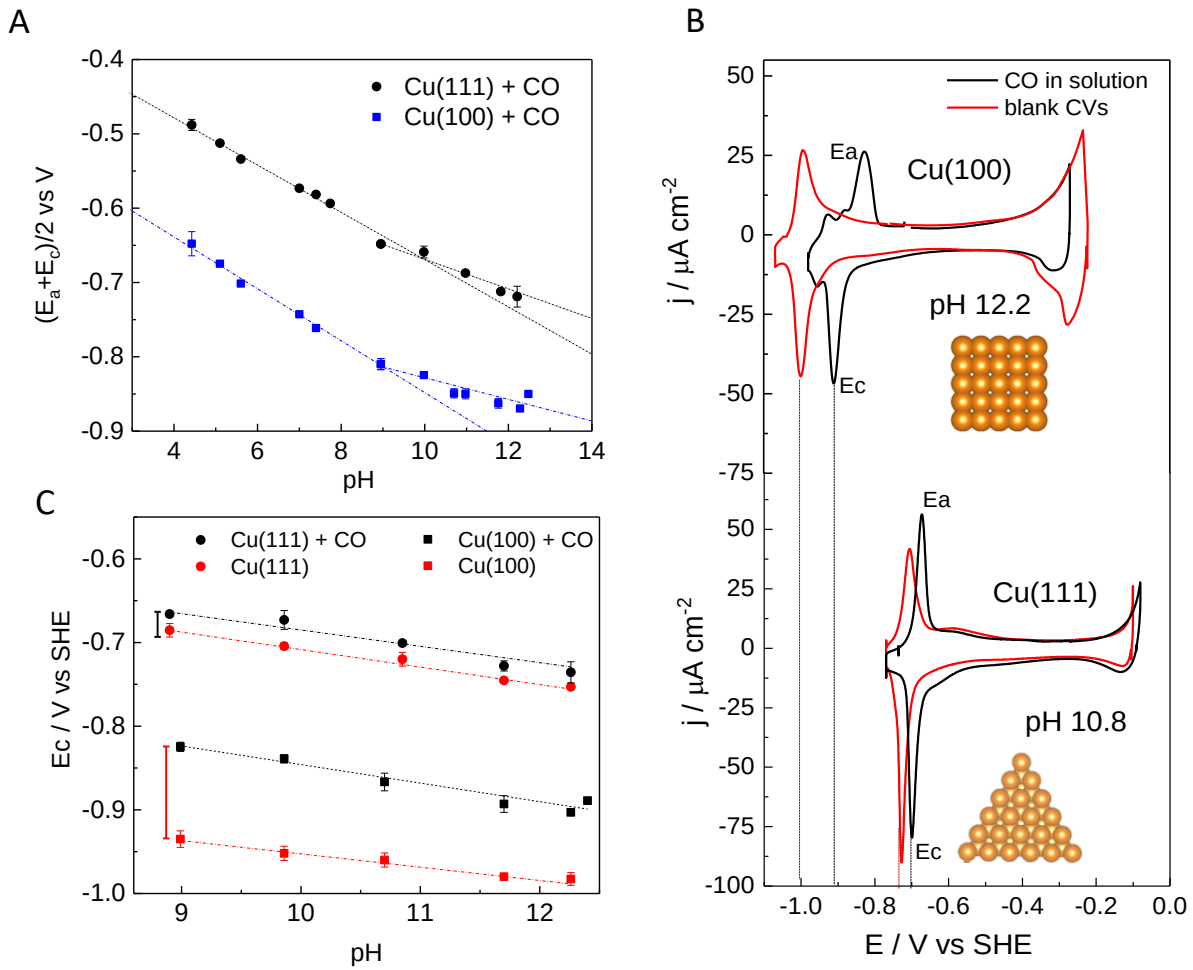

Figure 2: A) Plot of $(E_c-E_a)/2$ vs pH of both Cu(100) (blue squares) and Cu(111) (black circles) in phosphate buffer solutions and in presence of CO. B) C) Cyclic voltammograms of both Cu(111) and Cu(100) in red line) 0.1 M alkaline phosphate buffer solution, black line) same solution with CO. 50mV/s. C) Plot of the cathodic potential peak (E_c) vs pH in 0.1 M phosphate buffer solutions with CO (black symbols) and without CO (red symbols).

Experimental results were assessed under the lights of simulations of the interfacial region of Cu and the aqueous electrolyte, employing AIMD simulations of explicit electrolyte in contact with the surfaces. In the simulations of both Cu(100) and Cu(111) | phosphate electrolyte interface, the Cu surfaces were covered with H* and OH* from zero up to half coverage. Additionally, the

electrolyte was simulated with single H_xPO_4 anions, as well as with CO* and OCCOH* species adsorbed at the surface. In order to apply the generalized computational hydrogen electrode (GCHE) scheme, the work function and energy for each state from the AIMD simulations are saved. The GCHE scheme enables the explicit simulations of the interface phase diagrams, as the potential and the chemical potential of the ions are expressed by the work function and corresponding energetics. At each integer of pH, the most stable surface configurations were obtained by binning the work function in bins of a size of 0.02 eV. All GCHE energy states within each bin were Boltzmann-weighted. In Fig. 3A) and B), the coverage on Cu(100) (Fig. 3A) and on Cu(111) (Fig. 3B) of adsorbates are presented as a contour plot relative to the standard hydrogen electrode (U_{SHE}) potential and the pH. Each bin with a coverage above 0.1 monolayer of one of the CO*, OCCOH*, and H_xPO_4 adsorbates has been assigned with the respective color of the legend, whereas the varying coverages of H* and OH* are assigned with the color bar. The methodology of including phosphate anions in the GCHE has previously been applied for Cu[21] and is further elaborated in the S.I (Fig. S4 and S5). In summary, the methodology accounts for the phosphate reference to change concurrently with changes in pH, *i.e.* the phosphate species in the bulk electrolyte become less protonated with increasing pH. The change in phosphate reference is depicted in the S.I. (Fig. S5). The results from Fig. 3A) and B) show that in acidic and neutral pH, the Cu facets are covered with phosphate species up to high overpotentials, whereas at more alkaline conditions, the phosphate anions become unstable, leading to the CO* being adsorbed at an earlier potential. As the coverages of adsorbates change, a current (*j*) is generated. The currents were derived by the gradients of the coverages and are depicted in Fig. 3C) for Cu(100) and Fig. 3D) for Cu(111).

To investigate the shift in the CO peak, a Gaussian distribution is fitted to the current at every pH unity. The mean of each Gaussian distribution is also plotted in Fig. 3. The potential peak shift follows a linear trend with the pH, which resembles the experimental observed trends: as the pH increases, the CO surface poisoning shifts linearly to higher overpotentials, with a slope of 41 mV per pH unity. In contrast, at alkaline pH values, the potential peak shift with the pH is smaller, with a slope of 18 mV per pH unity for Cu(100) and 24.4 mV per pH unity for Cu(111), respectively. To rationalize the results from Fig. 3), a set of possible reactions of interchanging CO species with phosphate anions is proposed, as summarized in Table 1. From Fig. 3), the dominating CO* species differ on the two Cu facets, *i.e*. OCCOH* is adsorbed on Cu(100) and OCCO* is adsorbed on Cu(111). In addition to different CO species, the dominating phosphate anion species depend on the Cu facet as well: on the Cu(100) facet, HPO_4* is the dominating phosphate specie, whereas the adsorbed phosphate species changes on Cu(111) from HPO_4^* to PO_4* towards more neutral pHs (Fig. S6). As pH is increased, the adsorption occurring on the surface evolves from Eq. (1) towards Eq. (4), with Eq. (2) and Eq. (3) being the most predominant reactions in the pH range of the experiment. The charge of the adsorbed phosphate specie is not specified, inducing the *tilde* coefficients. Without the tilde, the coefficient of electrons would correspond to neutral charged phosphate species being adsorbed. The corresponding slopes are derived from the Nernst equation,[44] in the base-10 log form, at room temperature.

			Slope / [mV/pH]
Cu(100)	1	$H_3PO_4\ (aq) + OCCOH^* \rightarrow HPO_4^* + 2\ CO + 3\ H^+ + \sim 3\ e^-$	-59.2
	2	$H_2PO_4^-\ (aq) + OCCOH^* \rightarrow HPO_4^* + 2\ CO + 2\ H^+ + \sim 3\ e^-$	-39.5
	3	$PO_4^{2-}\ (aq) + OCCOH^* \rightarrow HPO_4^* + 2\ CO + H^+ + \sim 3\ e^-$	-19.7
	4	$PO_4^{3-}\ (aq) + OCCOH^* \rightarrow HPO_4^* + 2\ CO + \sim 3\ e^-$	0
Cu(111)	1	$H_3PO_4\ (aq) + OCCO^* \rightarrow PO_4^* + 2\ CO + 3\ H^+ + \sim 3\ e^-$	-59.2
	2	$H_2PO_4^-\ (aq) + OCCO^* \rightarrow PO_4^* + 2\ CO + 2\ H^+ + \sim 3\ e^-$	-39.5
	3	$HPO_4^{2-}\ (aq) + OCCO^* \rightarrow PO_4^* + 2\ CO + H^+ + \sim 3\ e^-$	-19.7
	4	$PO_4^{3-}\ (aq) + OCCO^* \rightarrow PO_4^* + 2\ CO + \sim 3\ e^-$	0

Table 1: a proposed set of equations of the adsorbate interchanging between the CO species and phosphate anions. The slopes are determined according to the Nernst equation, in the base-10 log form, at room temperature.

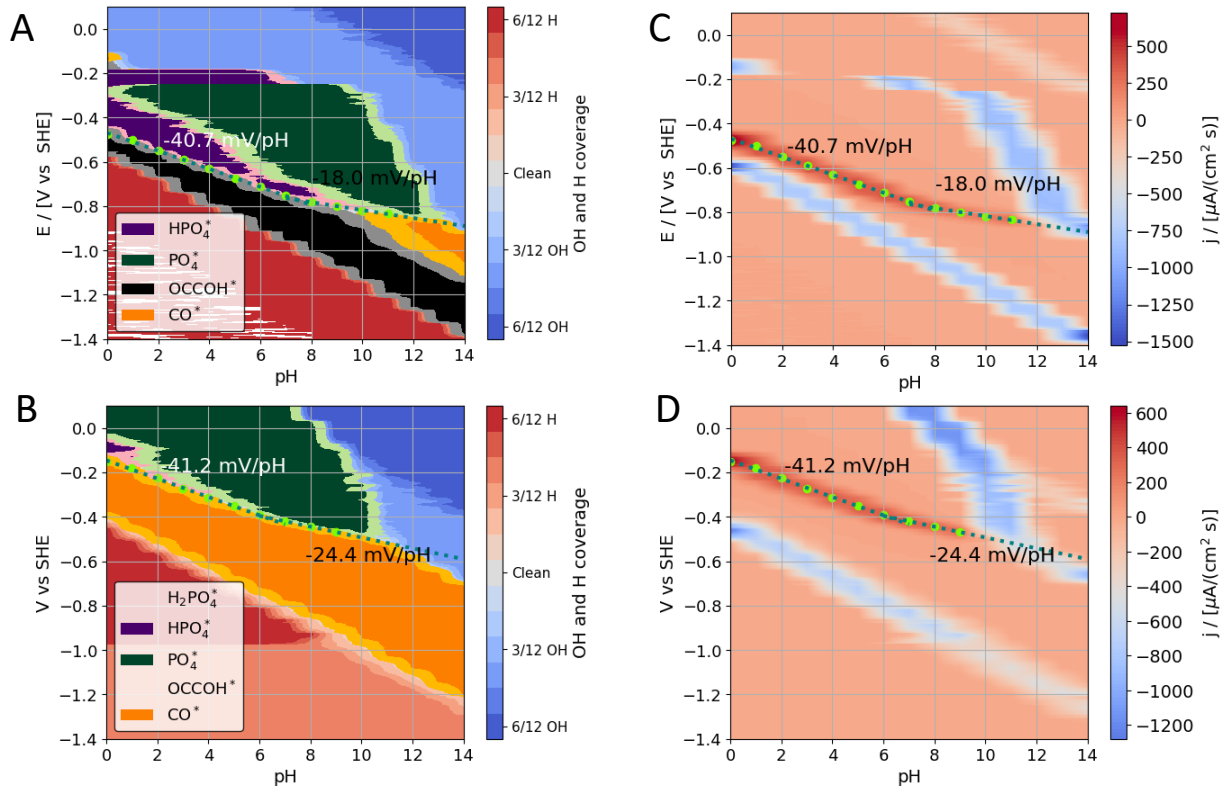

Figure 3: A and C show the interface Pourbaix diagrams of the most stable species on A) Cu(100) and B) Cu(111) as a function of pH and potential, calculated by Boltzmann-weighted binning of the energetics obtained by the GCHE scheme. C) and D) represent the current for Cu(100) and Cu(111), respectively, as a function of pH and potential as derived by the gradient of the Pourbaix diagram. The dotted lines are the means of the Gaussian distributions fitted to the current at each unity of pH.

To better compare experimental results with simulations, we have plotted, in Figure 4, the values of the averaged CO-potential peaks, ($\frac{Ea+Ec}{2}$), of Cu(100) and Cu(111) from the CVs in Fig 2, with the CO peak values extrapolated from simulations (Fig. 3).In both experiments and simulations, the CO adsorption on Cu(111) occurs at more positive potentials because of the weak anion binding on Cu(111), allowing H* to bind at more positive potentials and start evolving hydrogen

(HER). The experimental measurements show similar behavior in the difference between the peak shifts. However, when compared to the experimental results, the peak potentials for Cu(111) are shifted quite considerably to more positive values. This discrepancy might be due to different uncertainties, arising from the simulation model, *e.g*. the entropy of the adsorbed species at the surface is approximated to equal 0. Nonetheless, the main limitations of the simulation's validity arise from the limited number of included possible simulated interface structures and the corresponding sampled energetics. These limitations impose uncertainties on the coverages of the adsorbates, resulting in the uncertainties in the corresponding charge transfer and on set potentials.

Noteworthy, the slopes of the linear trends for the CO displacement peak originates from the anion reference and model itself, which omit the uncertainties from the simulations of specific coverages and energetics. The robustness by ± 0.5 eV of the anion reference is depicted in Figure S7. Despite the uncertainties with coverage and the phosphate anion reference, the overall phosphate electrolyte tendencies align with the experimental results obtained, and by previous observations made by Hori et al.[31,36] and in simulations.[22] Both experiments and simulations underline that the CO poisoning on Cu single-crystalline electrodes, is controlled by the specific properties of the Cu(hkl) | electrolyte interface.

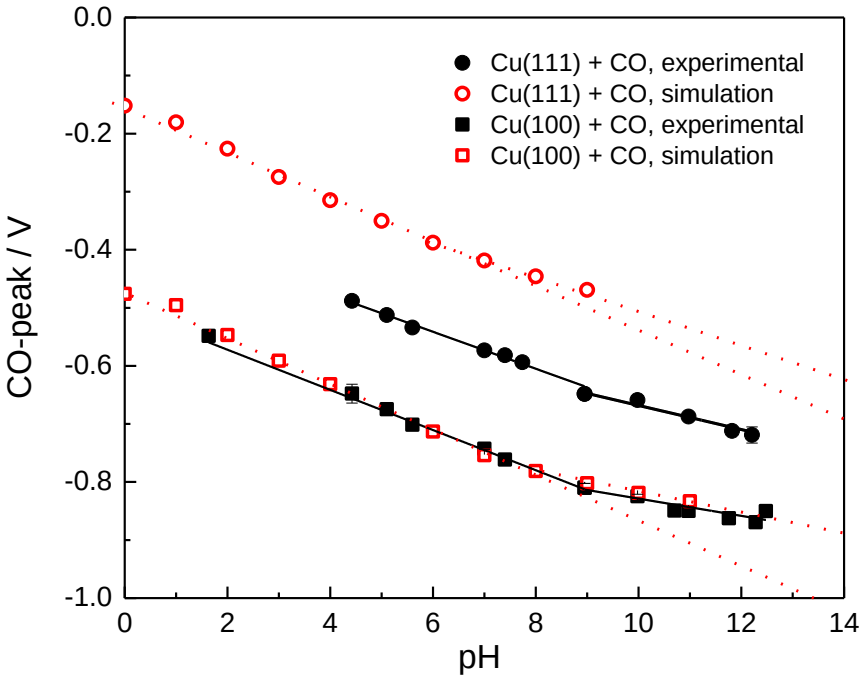

Figure 4: Plot of the CO-peaks as a function of the pH for black solid symbols) results obtained experimentally, red open symbols) from simulations of the Cu(hkl) | CO-saturated 0.1 M phosphate solution.

Conclusions

Herein we aimed to provide a detailed description of the structure of the interface between Cu(111) and Cu(100) | phosphate buffer solutions in presence of CO. The interfacial properties of the Cu(hkl)-electrolyte interface were assessed by combining voltammetric CO-displacement measurements and ab-initio simulations of the Cu single-crystalline electrodes-electrolyte interfaces. Good alignment was found between experiments and simulations, from which we showed that:

a) CO adsorbs on the surface in the potential region close to the desorption of phosphate anions from the electrolyte.

b) The adsorption of CO on Cu(111) take places at less negative potential values than on Cu(100) due to the lower binding energy of phosphate on Cu(111).

c) CO adsorption is stronger on Cu(100) than on Cu(111), shown by the more pronounced shift of the phosphate peaks CVs by CO on Cu(100) than on Cu(111), despite the fact that the phosphate adsorption on Cu(100) is stronger.

d) Experiments and simulation evidenced that the onset potential at which CO adsorbs on the surface is controlled by the properties of the Cu(hkl)-electrolyte interface.

In summary, this work highlights the importance of combining cyclic voltammetry under potential control with theoretical calculations to find the relations between interfacial properties of Cu electrodes and electrocatalytic CO reduction. Future work should be encouraged to elucidate and rationalize how specific electrolyte interactions and solvent reaction affect the surface structure stability of Cu-single crystalline surfaces under different potential conditions, as well as its influence on the CORR performance.

ASSOCIATED CONTENT

Detailed description of experimental details and computational details are included in the supporting information. Blank cyclic voltammograms of both Cu(111) and Cu(100) in phosphate buffer solutions, charge values and additional analysis of phosphate and CO peaks on both Cu facets are also included. The supporting information also contains the simulations of the Cu(111) and Cu(100) interfaces in contact with blank solutions.

AUTHOR INFORMATION

*Corresponding author:

E-mail: maria.escudero@chem.ku.dk

E-mail: alexander@chem.ku.dk

ORCID

Paula Sebastián-Pascual: 0000-0001-7985-0750

Alexander Bagger: 0000-0002-6394-029X

Jan Rossmeisl: 0000-0001-7749-6567

María Escudero-Escribano: 0000-0002-6432-3015

Notes

The authors declare no competing financial interest.

ACKNOWLEDGMENT

MEE and PSP gratefully acknowledge the Villum Foundation for the award of a Villum Young Investigator Grant (project number: 19142). We acknowledge support from VILLUM FONDEN, V-sustain grant 9455 and the Center of high entropy alloy catalysis, Danish national research foundation, DNRF-149.

References

(1) Chu, S.; Cui, Y.; Liu, N. The Path towards Sustainable Energy. *Nat. Mater.* **2016**, *16*, 16.

(2) De Luna, P.; Hahn, C.; Higgins, D.; Jaffer, S. A.; Jaramillo, T. F.; Sargent, E. H. What Would It Take for Renewably Powered Electrosynthesis to Displace Petrochemical Processes? *Science (80-.).* **2019**, *364* (6438), eaav3506.

(3) Eisenberg, R. Addressing the Challenge of Carbon-Free Energy. *ACS Energy Lett.* **2018**, *3* (7), 1521–1522.

(4) Nitopi, S. A.; Bertheussen, E.; Scott, S. B.; Liu, X.; Albert, K.; Horch, S.; Seger, B.; Stephens, I. E. L.; Chan, K.; Nørskov, J. K.; et al. Progress and Perspectives of Electrochemical CO_2 Reduction on Copper in Aqueous Electrolyte. *Chem. Rev.* **2019**, *119* (12), 610–7672.

(5) Gao, D.; Arán-Ais, R. M.; Jeon, H. S.; Roldan Cuenya, B. Rational Catalyst and Electrolyte Design for CO_2 Electroreduction towards Multicarbon Products. *Nat. Catal.* **2019**, *2* (3), 198–210.

(6) Sebastián-Pascual, P.; Mezzavilla, S.; Stephens, I. E. L.; Escudero-Escribano, M. Structure-Sensitivity and Electrolyte Effects in CO_2 Electroreduction: From Model Studies to Applications. *ChemCatChem* **2019**, *21* (0), 3626–3645.

(7) Kuhl, K. P.; Cave, E. R.; Abram, D. N.; Jaramillo, T. F. New Insights into the Electrochemical Reduction of Carbon Dioxide on Metallic Copper Surfaces. *Energy Environ. Sci.* **2012**, *5* (5), 7050–7059.

(8) Bagger, A.; Ju, W.; Varela, A. S.; Strasser, P.; Rossmeisl, J. Electrochemical CO_2 Reduction: A Classification Problem. *ChemPhysChem* **2017**, *18* (22), 3266–3273.

(9) Peterson, A. A.; Abild-Pedersen, F.; Studt, F.; Rossmeisl, J.; Nørskov, J. K. How Copper Catalyzes the Electroreduction of Carbon Dioxide into Hydrocarbon Fuels. *Energy Environ. Sci.* **2010**, *3* (9), 1311–1315.

(10) Hori, Y.; Murata, A.; Takahashi, R.; Suzuki, S. Electroreduction of CO to CH4and C2H4at a Copper Electrode in Aqueous Solutions at Ambient Temperature and Pressure. *J. Am. Chem. Soc.* **1987**, *109* (16), 5022–5023.

(11) Hori, Y.; Murata, A.; Yoshinami, Y. Adsorption of Carbon Monoxide, Intermediately Formed in Electrochemical Reduction of Carbon Dioxide, at a Copper Electrode. *J. Chem. Soc., Faraday Trans.* **1991**, *87* (Copyright (C) 2011 American Chemical Society (ACS). All Rights Reserved.), 125–128.

(12) Schouten, K. J. P.; Qin, Z.; Gallent, E. P.; Koper, M. T. M. Two Pathways for the Formation of Ethylene in CO Reduction on Single-Crystal Copper Electrodes. *J. Am. Chem. Soc.* **2012**, *134* (24), 9864–9867.

(13) Schouten, K. J. P.; Pérez-Gallent, E.; Koper, M. T. M. Structure Sensitivity of the Electrochemical Reduction of Carbon Monoxide on Copper Single Crystals. *ACS Catal.* **2013**, *3* (6), 1292–1295.

(14) Birdja, Y. Y.; Pérez-Gallent, E.; Figueiredo, M. C.; Göttle, A. J.; Calle-Vallejo, F.; Koper, M. T. M. Advances and Challenges in Understanding the Electrocatalytic Conversion of Carbon Dioxide to Fuels. *Nat. Energy* **2019**, *4* (9), 732–745.

(15) Rendón-Calle, A.; Builes, S.; Calle-Vallejo, F. A Brief Review of the Computational Modeling of CO_2 Electroreduction on Cu Electrodes. *Curr. Opin. Electrochem.* **2018**, *9*, 158–165.

(16) Hori, Y.; Takahashi, R.; Yoshinami, Y.; Murata, A. Electrochemical Reduction of CO at a Copper Electrode. *J. Phys. Chem. B* **1997**, *101* (36), 7075–7081.

(17) Hahn, C.; Hatsukade, T.; Kim, Y.-G.; Vailionis, A.; Baricuatro, J. H.; Higgins, D. C.; Nitopi, S. A.; Soriaga, M. P.; Jaramillo, T. F. Engineering Cu Surfaces for the Electrocatalytic Conversion of CO_2 : Controlling Selectivity toward Oxygenates and Hydrocarbons. *Proc. Natl. Acad. Sci.* **2017**, *114* (23), 5918–5923.

(18) Pérez-Gallent, E.; Marcandalli, G.; Figueiredo, M. C.; Calle-Vallejo, F.; Koper, M. T. M. Structure- and Potential-Dependent Cation Effects on CO Reduction at Copper Single-Crystal Electrodes. *J. Am. Chem. Soc.* **2017**, *139* (45), 16412–16419.

(19) Huang, Y.; Handoko, A. D.; Hirunsit, P.; Yeo, B. S. Electrochemical Reduction of CO2 Using Copper Single-Crystal Surfaces: Effects of CO* Coverage on the Selective Formation of Ethylene. *ACS Catal.* **2017**, *7* (3), 1749–1756.

(20) Arán-Ais, R. M.; Scholten, F.; Kunze, S.; Rizo, R.; Roldan Cuenya, B. The Role of in Situ Generated Morphological Motifs and Cu(i) Species in C2+ Product Selectivity during CO2 Pulsed Electroreduction. *Nat. Energy* **2020**, DOI: 10.1038/s41560-020-0594-9.

(21) Tiwari, A.; Heenen, H. H.; Bjørnlund, A. S.; Maagaard, T.; Cho, E.; Chorkendorff, I.; Kristoffersen, H. H.; Chan, K.; Horch, S. Fingerprint Voltammograms of Copper Single Crystals under Alkaline Conditions: A Fundamental Mechanistic Analysis. *J. Phys. Chem.*

Lett. **2020**, *11* (4), 1450–1455.

(22) Bagger, A.; Arnarson, L.; Hansen, M. H.; Spohr, E.; Rossmeisl, J. Electrochemical CO Reduction: A Property of the Electrochemical Interface. *J. Am. Chem. Soc.* **2019**, *141* (4), 1506–1514.

(23) Sebastián-Pascual, P.; Escudero-Escribano, M. Addressing the Interfacial Properties for CO Electroreduction on Cu with Cyclic Voltammetry. *ACS Energy Lett.* **2020**, *5* (1), 130–135.

(24) Le Duff, C. S.; Lawrence, M. J.; Rodriguez, P. Role of the Adsorbed Oxygen Species in the Selective Electrochemical Reduction of CO_2 to Alcohols and Carbonyls on Copper Electrodes. *Angew. Chemie - Int. Ed.* **2017**, *56* (42), 12919–12924.

(25) Bagger, A.; Arán-Ais, R. M.; Halldin Stenlid, J.; dos Santos, E.; Arnarson, L.; Degn Jensen, K.; Escudero-Escribano, M.; Roldan Cuanya, B.; Rossmeisl, J. Ab Initio Cyclic Voltammetry on Cu(111), Cu(100) and Cu(110) in Acidic, Neutral and Alkaline Solutions. *ChemPhysChem* **2019**, *20* (0), 1–11.

(26) Bagger, A.; Ju, W.; Varela, A. S.; Strasser, P.; Rossmeisl, J. Electrochemical CO_2 Reduction: Classifying Cu Facets. *ACS Catal.* **2019**, *9* (9), 7894–7899.

(27) Varela, A. S.; Kroschel, M.; Reier, T.; Strasser, P. Controlling the Selectivity of CO_2 electroreduction on Copper: The Effect of the Electrolyte Concentration and the Importance of the Local PH. *Catal. Today* **2016**, *260*, 8–13.

(28) Stenlid, J. H.; Dos Santos, E. C.; Bagger, A.; Johansson, A. J.; Rossmeisl, J.; Pettersson,

L. G. M. Electrochemical Interface during Corrosion of Copper in Anoxic Sulfide-Containing Groundwater—A Computational Study. *J. Phys. Chem. C* **2020**, *124* (1), 469–481.

(29) Ooka, H.; Figueiredo, M. C.; Koper, M. T. M. Competition between Hydrogen Evolution and Carbon Dioxide Reduction on Copper Electrodes in Mildly Acidic Media. *Langmuir* **2017**, *33* (37), 9307–9313.

(30) Varela, A. S. The Importance of PH in Controlling the Selectivity of the Electrochemical CO_2 Reduction. *Curr. Opin. Green Sustain. Chem.* **2020**, 100371.

(31) Koga, O.; Watanabe, Y.; Tanizaki, M.; Hori, Y. Specific Adsorption of Anions on a Copper (100) Single Crystal Electrode Studied by Charge Displacement by CO Adsorption and Infrared Spectroscopy. *Electrochim. Acta* **2001**, *46* (20–21), 3083–3090.

(32) Jensen, K. D.; Tymoczko, J.; Rossmeisl, J.; Bandarenka, A. S.; Chorkendorff, I.; Escudero-Escribano, M.; Stephens, I. E. L. Elucidation of the Oxygen Reduction Volcano in Alkaline Media Using a Copper–Platinum(111) Alloy. *Angew. Chemie - Int. Ed.* **2018**, *57* (11), 2800–2805.

(33) Dong, J.-C.; Zhang, X.-G.; Briega-Martos, V.; Jin, X.; Yang, J.; Chen, S.; Yang, Z.-L.; Wu, D.-Y.; Feliu, J. M.; Williams, C. T.; et al. In Situ Raman Spectroscopic Evidence for Oxygen Reduction Reaction Intermediates at Platinum Single-Crystal Surfaces. *Nat. Energy* **2019**, *4* (1), 60–67.

(34) Gómez-Marín, A. M.; Rizo, R.; Feliu, J. M. Oxygen Reduction Reaction at Pt Single Crystals: A Critical Overview. *Catal. Sci. Technol.* **2014**, *4* (6), 1685–1698.

(35) Strmcnik, D.; Escudero-Escribano, M.; Kodama, K.; Stamenkovic, V. R.; Cuesta, A.; Marković, N. M. Enhanced Electrocatalysis of the Oxygen Reduction Reaction Based on Patterning of Platinum Surfaces with Cyanide. *Nat. Chem.* **2010**, *2*, 880.

(36) Hori, Y.; Koga, O.; Watanabe, Y.; Matsuo, T. FTIR Measurements of Charge Displacement Adsorption of CO on Poly- and Single Crystal (100) of Cu Electrodes. *Electrochim. Acta* **1998**, *44* (8–9), 1389–1395.

(37) Koga, O.; Matsuo, T.; Hoshi, N.; Hori, Y. Charge Displacement Adsorption of Carbon Monoxide on [110] Zone Copper Single Crystal Electrodes in Relation with PZC. *Electrochim. Acta* **1998**, *44* (6–7), 903–907.

(38) Martínez-Hincapié, R.; Sebastián-Pascual, P.; Climent, V.; Feliu, J. M. Exploring the Interfacial Neutral PH Region of Pt(111) Electrodes. *Electrochem. commun.* **2015**, *58*, 62–64.

(39) Ganassin, A.; Sebastián, P.; Climent, V.; Schuhmann, W.; Bandarenka, A. S.; Feliu, J. On the pH Dependence of the Potential of Maximum Entropy of Ir(111) Electrodes. *Sci. Rep.* **2017**, *7* (1), 1246.

(40) Kim, Y.-G.; Javier, A.; Baricuatro, J. H.; Torelli, D.; Cummins, K. D.; Tsang, C. F.; Hemminger, J. C.; Soriaga, M. P. Surface Reconstruction of Pure-Cu Single-Crystal Electrodes under CO-Reduction Potentials in Alkaline Solutions: A Study by Seriatim ECSTM-DEMS. *J. Electroanal. Chem.* **2016**, *780*, 290–295.

(41) Matsushima, H.; Taranovskyy, A.; Haak, C.; Gründer, Y.; Magnussen, O. M. Reconstruction of Cu(100) Electrode Surfaces during Hydrogen Evolution. *J. Am. Chem.*

Soc. **2009**, *131* (30), 10362–10363.

(42) Kim, Y. G.; Baricuatro, J. H.; Javier, A.; Gregoire, J. M.; Soriaga, M. P. The Evolution of the Polycrystalline Copper Surface, First to Cu(111) and Then to Cu(100), at a Fixed CO_2RR Potential: A Study by Operando EC-STM. *Langmuir* **2014**, *30* (50), 15053–15056.

(43) Grunder, Y.; Beane, J.; Kolodziej, A.; Lucas, C. A.; Rodriguez, P. Potential Dependent Structure and Stability of Cu(111) in Neutral Phosphate Electrolyte. *Surfaces* **2019**, *2* (1), 145–158.

(44) Bard, A. J.; Faulkner, L. R. *Electrochemical Methods : Fundamentals and Applications /*, 2. ed.; Bard, A. J., Faulkner, L. R., Eds.; John Wiley: New York.